SISSA

PAPER • OPEN ACCESS

Exploring the potential of muon radiography for blast furnace assessments: advancements in non-invasive imaging and structural analysis

To cite this article: C. Frosin *et al* 2024 *JINST* **19** C02041

View the article online for updates and enhancements.

16TH TOPICAL SEMINAR ON INNOVATIVE PARTICLE AND RADIATION DETECTORS
SIENA, ITALY
25–29 SEPTEMBER 2023

Exploring the potential of muon radiography for blast furnace assessments: advancements in non-invasive imaging and structural analysis

The BLEMAB collaboration

C. Frosin,[a,b,*] F. Ambrosino,[c,d] P. Andreetto,[e] L. Bonechi,[b] G. Bonomi,[f,g]
D. Borselli,[a,h] S. Bottai,[b] T. Buhles,[i] I. Calliari,[j] P. Checchia,[e] U. Chiarotti,[k]
C. Cialdai,[b] R. Ciaranfi,[b] L. Cimmino,[c,d] V. Ciulli,[a,b] P.G. De Seta Cosentino,[l]
R. D'Alessandro,[a,b] R.P. Santos Ferreira,[l] F. Finke,[i] A. Franzen,[i] B. Glaser,[m]
S. Gonzi,[a,b] A. Lorenzon,[n,e] V. Masone,[d] V. Moroli,[k] O. Nechyporuk,[l] A. Paccagnella,[a,b]
R. Petrini,[b] L. Pezzato,[j] B.V. Rangavittal,[m] D. Ressegotti,[o] G. Saracino,[c,d]
J. Sauerwald,[i] O. Starodubtsev,[b] L. Viliani,[b] F. Volzone[k] and M. Vynnycky[m]

[a]*Department of Physics and Astronomy, University of Florence,*
 Via Giovanni Sansone 1, 50019 Sesto Fiorentino, Italy

[b]*INFN Florence,*
 Via Bruno Rossi, 1, 50019 Sesto Fiorentino, Italy

[c]*Physics Department "Ettore Pancini", University of Naples Federico II,*
 Via Cintia, 21 - Building 6, 80126 Naples, Italy

[d]*INFN Naples,*
 Via Cintia, 21, 80126 Naples, Italy

[e]*INFN Padua,*
 Via Francesco Marzolo, 8, 35131 Padua, Italy

[f]*Department of Mechanical and Industrial Engineering, University of Brescia,*
 Via Branze, 38, 25123 Brescia, Italy

[g]*INFN Pavia,*
 Via Agostino Bassi, 6, 27100 Pavia, Italy

*Corresponding author.

^{h}*Department of Physics and Geology, University of Perugia,*
  Via Alessandro Pascoli, 06123 Perugia, Italy

^{i}*Ironmaking Department, ArcelorMittal Bremen GmbH,*
  Auf den Delben 35, 28237 Bremen, Germany

^{j}*Department of Industrial Engineering, University of Padua,*
  Via Marzolo 9, 35131 Padua, Italy

^{k}*Rina Consulting — Centro Sviluppo Materiali SpA,*
  via Castel Romano 100, 00128 Rome, Italy

^{l}*Ironmaking department, ArcelorMittal Maizières Research,*
  Voie Romaine, 57280 Maizières-lès-Metz, France

^{m}*Division of Processes, Department of Materials Science and Engineering, KTH Royal Institute of Technology,*
  Brinellvagen 23, 100 44 Stockholm, Sweden

^{n}*Department of Physics and Astronomy, University of Padua,*
  Via Francesco Marzolo, 8, 35131 Padua, Italy

^{o}*Rina Consulting — Centro Sviluppo Materiali SpA,*
  Viale Lombardia, 24044 Dalmine (BG), Italy

E-mail: catalin.frosin@unifi.it

ABSTRACT: The BLEMAB European project (BLast furnace stack density Estimation through online Muon ABsorption measurements), the evolution of the previous Mu-Blast European project, is designed to investigate in detail the capability of muon radiography techniques applied to the imaging of the inner zone of a blast furnace. In particular, the goal of this collaboration is to characterize the internal region (so-called cohesive zone) where the slowly downward-moving material begins to soften and melt, which plays an important role in the performance of the blast furnace itself. In this contribution, we describe the state-of-the-art of the muon tracking system which is currently being developed and installed at a blast furnace on the ArcelorMittal site in Bremen (Germany). Moreover, we will present the GEANT4 simulation framework devised for this application together with the simulation results. Finally, we will show the possible contribution of multiple scattering effects to such peculiar applications.

Contents

1 Introduction to muon radiography

Based on the usage of the natural muon flux continuously produced by high-energy cosmic rays in the Earth's atmosphere (see for example [1–3]), muon transmission radiography (also called muography) is a non-invasive survey technique that can be used in many fields, from archaeology to civil engineering, from mining to volcanology. This technique provides precise information on the two-dimensional average density distribution of very thick material layers up to hundreds of meters. For this reason, it represents a powerful tool complementary or alternative to other more common survey methods, particularly in cases where the material thicknesses are too large or the volume to be measured is not accessible.

The next two paragraphs provide an introduction to the muon transmission radiography technique and the imaging methodology.

1.1 Muon radiography

Like electrons, muons are charged elementary particles belonging to the Lepton family. Muons are continuously produced in the upper layer of the Earth's atmosphere due to the collisions of very high-energy cosmic rays. The primary cosmic ray gives origin to different particles (also called *particle showers*) amongst which we find kaons and pions primarily responsible through their decay for the muon production.

Thanks to the high energies at production and their large mass, atmospheric muons can reach the earth's surface and even penetrate up to hundreds of meters of rock. In fact, the muon flux represents the most abundant component at sea level of the secondary cosmic ray flux. For example, the integrated vertical flux at sea level above 1 GeV is about $70\,\mathrm{m^{-2}\,sr^{-1}\,s^{-1}}$. Taking into account all zenith angles, the muon flux can be described by a $cos(\theta)^n$ distribution, where $n \sim 2$ has a

slight dependence on energy. Therefore, for a fixed energy and azimuth angle ϕ, the flux is the highest for $\theta = 0°$ and lowest for $\theta = 90°$. Moreover, the differential flux at high angles is also shifted towards higher energies as the atmospheric depth seen by the muons is bigger and thus the low-energy component has a higher decay probability. In the following, we will use the zenith-azimuth or elevation-azimuth (defined as $e = 90° - \theta$) coordinates.

The basic idea of muography is to exploit this natural atmospheric muon flux to perform radiographic studies of large massive structures, thus mimicking what is usually done with X-rays in medical applications. Detailed reviews about muon imaging and the relative instrumentation can be found in [2, 3].

1.2 Image reconstruction in muography

To fully reconstruct a muographic image (i.e. a directional density map) one needs in general to follow four steps consisting of two measurements and two simulations. The two measurements represent the target measurement where the object to investigate is between the source and detector and the free sky measurement of the flux without the object. The result of these two steps is the measurement of the directional transmission of the muons; the fraction of incoming muons that is able to cross the thickness of the material encountered along one direction.

Successively, the interpretation of the measured transmission requires a comparison with simulations that must consider the geometry of the volume under examination (i.e DTM[1] or CAD models), the characteristics of the muon flux and the other information available on the material structures placed in the acceptance of the experimental apparatus used for the measurement. Therefore, one can proceed to perform a target simulation implementing the same setup as the target measurement and a freesky simulation following a muon generator. Many generators and experimental measurements can be found in the literature describing muon flux at ground level (see [4]), but often these are not sufficiently accurate or complete to fully describe the energy and angular ranges required for our muon radiography applications. The INFN-UNIFI team in Florence has measured muon energy and angular spectra at ground level in the momentum range from 0.1 to 130 GeV/c and in the zenith angle range from 0° up to 80° using the ADAMO [5] magnetic spectrometer made with a permanent magnet and a microstrip silicon tracker. Based on these measurements, a fast muon generator was implemented and successfully used to compare different muon radiographs with dedicated simulations [7–9]. The spectrometer results have been used for the implementation of a realistic atmospheric muon generator integrated within a GEANT4 software package which will be described in a future dedicated article.

The next step is to build the so-called relative transmission (R). This quantity represents the ratio between the measured and simulated transmission. If for a line of sight (θ,ϕ), $R = 1$ the simulated density matches the measured one while if $R > (<)1$ the mean measured density is lower (higher) than the simulated one. By repeating the simulation with different density hypotheses, we can build a density map where for each bin we choose the density ρ in order to have $R = 1$. Finally, by combining multiple measurements performed from different viewpoints, information on the three-dimensional density distribution can be derived.

---

[1]Digital Terrain Model.

2 The BLEMAB project and detector

A blast furnace is a continuously operating shaft furnace based on the counter-current flow principle. At the top coke and burden (pellets and lump iron ore) are charged in alternating layers. In the lower part of the furnace, hot blast from hot stoves is injected through tuyeres. In front of each tuyere, the hot blast reacts with the coke. Carbon monoxide is formed, and it ascends in the furnace and reduces the iron oxides in the ferrous ores. At the bottom of the hearth, the molten metal is collected. See [9] and references therein for a complete description. Generally, retrieving information on the reduction process during operation is strongly hindered by the harsh environment inside the blast furnace (high temperature and pressure). Material distributions or data about reaction parameters can be obtained only at downtimes with core drilling or by dissection at the end of the lifespan of the furnace. The new muography approach within the BLEMAB (BLast furnace stack density Estimation through online Muon ABsorption measurements) project [10] is investigated in order to overcome these limitations. A similar study was proposed in 2005 [11] and more recently a muon tomographic technique was also applied [12].

2.1 The BLEMAB detector

The muon transmission radiography requires the installation of at least one muon tracking system downstream of the volume of interest. For the BLEMAB project, two independent muon trackers have been realized to have the possibility of installing them either both in the same blast furnace (stereoscopic view) or one in front of a blast furnace and the other in an open space for the freesky reference measurement. The third option is to place the detectors into two different blast furnaces to perform a comparative study of their internal structures.

Each of the trackers is made of three independent $80 \, \text{cm} \times 80 \, \text{cm}$ tracking modules measuring two coordinates of muon impact position along two orthogonal axes (XY). The tracking modules are based on the same technology used for the MURAVES [13] and MIMA [14] projects. Each XY tracking module is composed of orthogonal tracking planes each consisting of 64 scintillator bars, $80 \, \text{cm}$ long, with triangular section. The scintillator material is a fast organic polystyrene-based plastic, characterized by large bulk attenuation length, large light yield and small signal rise time.
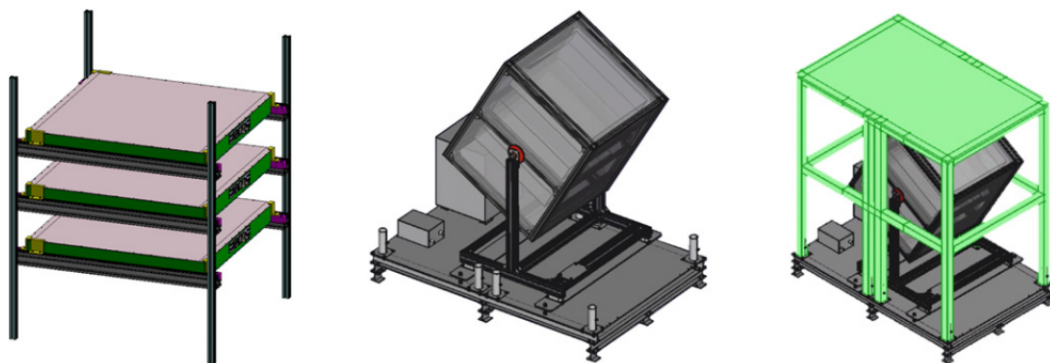

Figure 1. Left: single BLEMAB tracker, composed of three XY tracking modules. Centre: the BLEMAB tracker was installed on its mounting and placed on the base plate. Right: the skeleton of the protection frame with a steel cover plate at its top (in green). Reproduced from [10]. © 2022 IOP Publishing Ltd and Sissa Medialab. All rights reserved.

Each scintillator bar is read by means of two silicon photomultipliers with an area of $4 \times 4\,\mathrm{mm}^2$. The tracking module has inside an acquisition system made of four custom DAQ slave boards housing an EASIROC1B 32 channels front-end chip and an ASIC to control the front-end circuitry and the transmission of data to a central custom DAQ master board. The latter implements the trigger logic and manages the data collection from up to 16 slave boards. A Raspberry PI computer, connected to the master DAQ board, is used to set the whole electronic chain, receive the data packet from the master DAQ board and write it to a physical support. Network access to the detector is available through a SIM-operated commercial modem. This allows the online detector control and data synchronisation to a remote server.

A single muon tracking detector (three XY modules) is enclosed in a light aluminium box and fixed on a custom mounting which allows for remote modification of the detector's pointing direction. The whole measuring system will be housed inside a large metal frame (see right side of figure 1), covered by metal panels, to protect the apparatus from possible blows, splashes of liquids and corrosive vapours. The drawings of the detector and the housing frame are shown in figure 1. Because the blast furnace's environment can reach quite high temperatures, a conditioner cooling system has been installed inside the same protection box, in order not to have strong variations in the working temperature of the optical sensors.

2.2 The installation site

The installation of the detection system (BLEMAB01 and BLEMAB02 trackers hereafter) took place in August 2023. The measurement focuses on the study of blast furnace No.2 of ArcelorMittal Bremen as it was previously done in a preliminary study by [15]. The structure is approximately 40 m in height and has a radius of up to 16 m at the tuyere level. In figure 2 on the left, a picture taken during the movement of the two detectors at the base of the blast furnace is shown. On the right side, a schematization of the final configuration with the actual positioning of the trackers is represented. BLEMAB01 is pointing with an elevation of 47° at the centre of the furnace and it is placed at the base level. On the other hand, due to operational requirements and space occupancy of the whole detection system, BLEMAB02 had to be placed on a higher level just underneath the tuyere pointing at the same elevation as BLEMAB01. The dotted lines show the pointing of the centre of the two
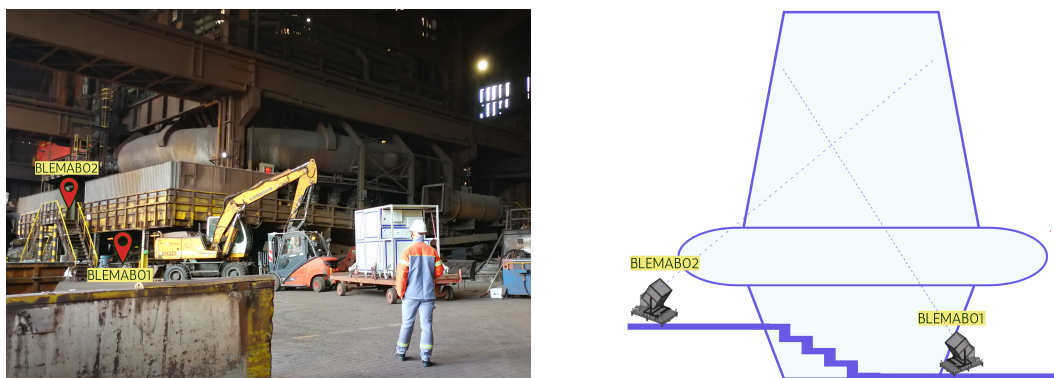

Figure 2. Left: installation points to the blast furnace underneath the walkway, corresponding to BLEMAB01 and at the tuyere level corresponding to BLEMAB02. Right: schematic representation of the actual position of the two detectors pointing at 47° in elevation in the direction of the blast furnace.

detectors. The elevation was chosen in order to see most of the cohesive region and to match the freesky measurement done the previous month in the same place but without any object in the field of view of the detector. The pointing system can be operated remotely and only the levelling to the ground surface must be done in place by means of adjustable feet at the base of the detector housing. Currently, the data taking is still ongoing and by the end of this year, the measurement of blast furnace No.2 of ArcelorMittal Bremen will be completed, taking reference data also during a shutdown.

3 Results of the preliminary simulations

Before the data analysis, a preliminary simulation phase has been performed. One of the goals was to study the possible effect of multiple scattering (MS) on the muography map and to the specific application to blast furnaces. In fact, it is known as shown in [16], that depending on the type of measurement, MS can or cannot be negligible and must be evaluated for each case study.

3.1 The simulation framework

For our simulation, we used a GEANT4-based [17] framework where different configurations have been investigated as shown in figure 3. The standard *emstandard* with *opt4* physics constructor was employed as it is suggested to be used for applications that require higher accuracy of electrons, hadrons and ion tracking. For more details on the implementation with a particular focus on the MS see [18, 19] and references therein.
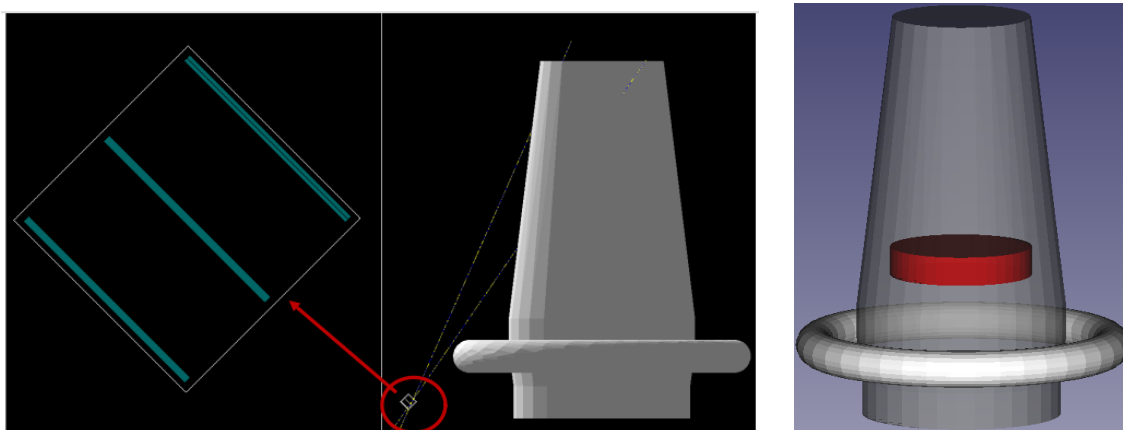
Figure 3. Left: configuration A (full Fe blast furnace) of the geometry used in the simulation including a zoom of the detector geometry with a see-thru of the tracking planes. Right: configuration B (cohesive zone mock-up as a red plate) of the geometry used in the simulation. See the text for the details.

The first simulation regarded the estimation of the MS effect in the case of a full Fe blast ($\rho = 7.87 \, \text{g/cm}^3$) furnace as the worst-case scenario (left side of figure 3). In the second case, we simulated a low-density region ($\rho = 3.94 \, \text{g/cm}^3$) inside the Fe blast furnace to see the variation in muon counts that can be produced by a region like the cohesive zone. The plate-like geometry (right side of figure 3) is a simplification and in the future a more precise material distribution will be implemented. In fact, the cohesive zone is expected to have more of an upside-down "V" shape which in certain cases can evolve into a "W". The geometry of the detector is implemented using a CAD containing the different parts which can then be treated separately in terms of density.

The detector is reproduced in its actual internal structure, having the 80 cm long triangular shape bars in each XY module. However, the protection box has not yet been fully integrated into the simulation and it is not considered in the following results. For the simulation, the detector has been placed 15 m away from the furnace pointing at 47° at the same height as BLEMAB02. The muon source is modelled following the ADAMO detector [5] data and the simulation is run in the $0.3 < p < 500$ GeV/c momentum range and over the full θ and ϕ phase space.

3.2 Multiple scattering effects

When muons cross materials, their trajectories are continuously modified due to the random electromagnetic interactions with the charged nuclei and to a lesser degree with the electrons of the medium. The final effect is an overall deflection of the trajectory with respect to the original one. The intensity of this effect is higher for low-energy particles and increases with the atomic number Z of the traversed medium. This dependence is the key feature behind the multiple scattering muon tomography technique [3, 20].

The blast furnace is a high Z material which can enhance the effect of MS but the overall effect is also influenced by the geometry and measurement configuration as pointed out by [16]. One would expect that certain muons are deflected away from the detector (out-scattering) thus reducing the measured muon flux from the observed direction. Additionally, there would also be a part of the muon flux that would initially not hit the detector if the muons were to propagate on a perfectly straight trajectory but are deflected into the detector. This so-called in-scattering would then increase the muon flux from the apparent incidence direction of the muon (assuming a straight path). For the case of an underground measurement or a detector surrounded by material in- and out-scattering usually cancel each other out and do affect muographic measurements only through a "blurring" effect. In the case of a muon flux measurement near an object with portions of the freesky directly seen by the detector, the situation is instead different. There can be an imbalance between in- and out-scattering muons due to a non-symmetric configuration. For example, one might observe a too-high muon flux around the edges of the target.
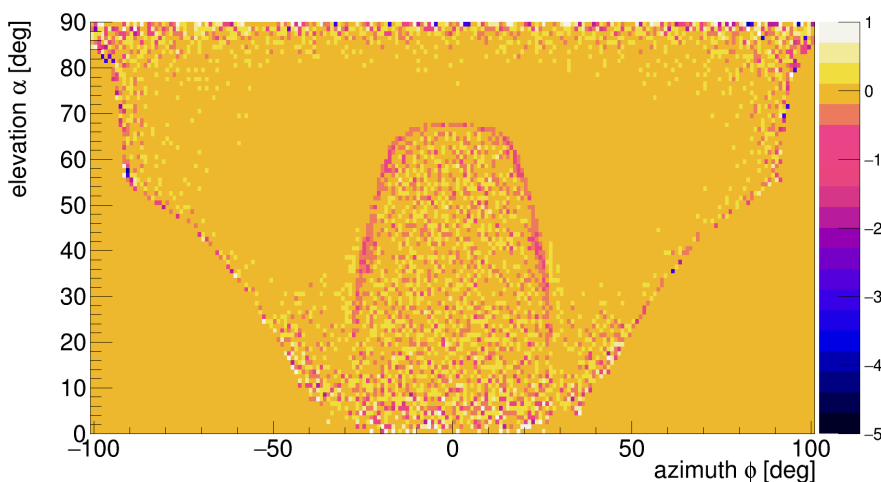

Figure 4. Azimuth-elevation map obtained by plotting the difference between generation and detection counts divided by the generation counts.

Indeed, this is what we observe in the blast furnace case as shown in figure 4. Here it is shown the azimuth-elevation map of the difference between generation and detection counts divided by the generation counts. Values equal to zero indicate no scattering, values greater than zero indicate fewer muons detected than the ones generated and values smaller than zero indicate that more muons are detected than the ones generated in a certain angular bin. As one can notice from figure 4, there is a strong component of deflection present on the skin of the blast furnace which can be clearly recognized as it highlights the borders of the object. This is determined by the in-going muons that end up being detected even if the original straight path was not lying inside the detector's acceptance but which due to MS are nevertheless detected.

In order to give a quantitative description of this phenomenon, we built up the following observable:

$$\theta_{\text{msc}} = \arccos \frac{\vec{p}_{\text{det}} * \vec{p}_{\text{gen}}}{p_{\text{det}} * p_{\text{gen}}} \tag{3.1}$$

where $\vec{p}_{\text{det}}$, $\vec{p}_{\text{gen}}$, p_{det} and p_{det} are the momenta of the detected and generated muons and their magnitude, respectively. This variable describes the overall deflection of the muon with respect to their direction at the source. If no multiple scattering effects were present then this variable should be zero. The freesky and target measurement distributions are shown in figure 5 as a function of the detected momentum. As one can see, already in the freesky we observe a small part of muons with a non-negligible deflection, implying that the detector itself plays a role especially if we detect also the low energy (<1 GeV/c) component of the muon flux.

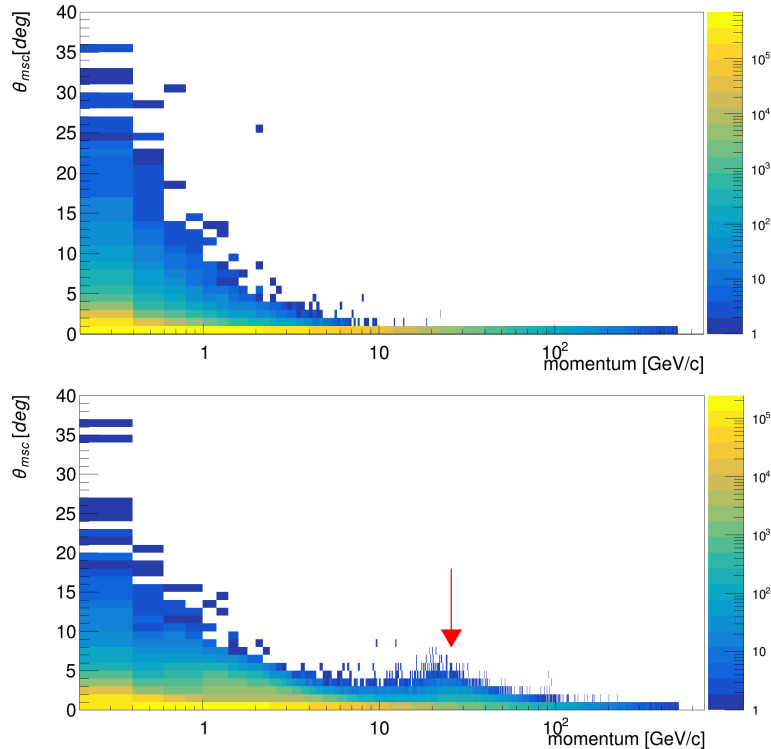**Figure 5.** Top: the θ_{msc} variable is plotted as a function of the detected momentum of the muons for the freesky measurement, highlighting the presence of the MS inside the detector. Bottom: the same plot as on the left but this time with the target in front of the detector. The red arrow points out the target contribution region. The X-axis is plotted in logarithmic scale.

On the other hand, at the bottom of figure 5, one can also distinguish a contribution from the blast furnace (red arrow). Since the detector has an angular resolution of about 1°, we can consider as significant the muons above this threshold in the previous plots to have a rough estimate from the different multiple scattering components. We estimated that 1.60%±0.01% of the detected muons have undergone significant deflections, considering both the target and detector contributions. Additionally, 4.76%±0.04% of the generated muons were lost (deflected from the detector's acceptance) due to the multiple scattering contributions. This has been estimated by turning off the MS processes in the Geant4 simulation.

3.3 Preliminary map

As described in the simulation framework, in the second configuration we simulated a low-density region inside the blast furnace to see the variation in muon counts and thus in transmission, that can be produced by a region like the cohesive zone. The results are shown in figure 6 where the complete transmission map and a zoom around the corresponding low-density zone are depicted. The shadow of the blast furnace can be recognized together with the hot air blast torus surrounding the bottom area of the object. In these plots, green areas represent the region where the freesky is seen directly, as the transmission values are by definition the ratio between the muon flux with and without the target. The
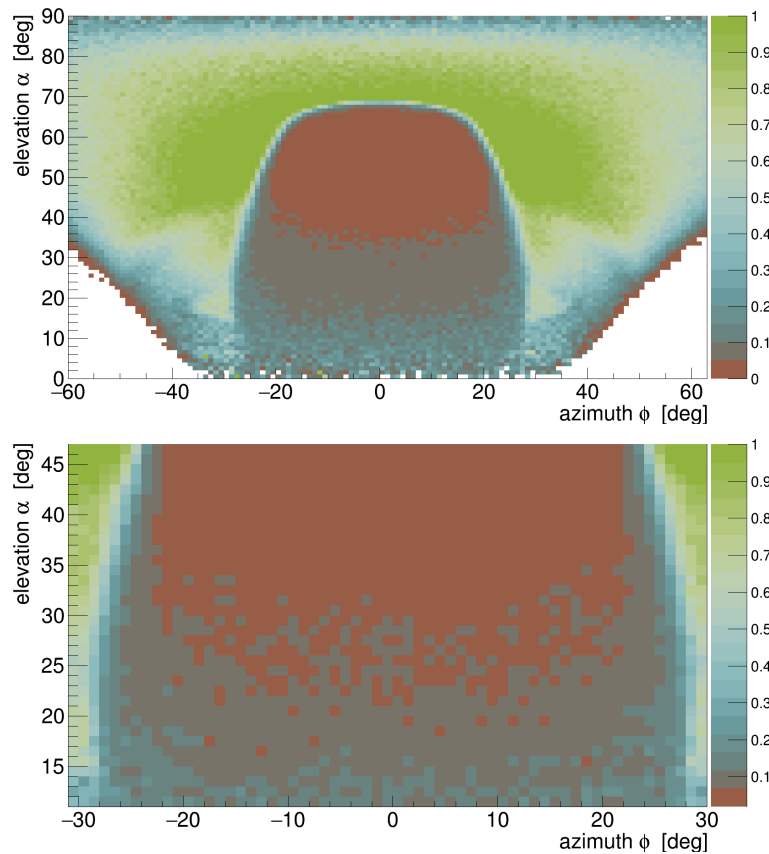

Figure 6. Top: simulated transmission map for the second configuration shown in figure 2 where the cohesive zone is placed as a low-density plate inside the blast furnace. Bottom: zoom of the top figure in the elevation-azimuth region corresponding to the cohesive zone.

darker region represents the blast furnace area where the muon flux is much lower with respect to the freesky. As shown by the bottom plot of figure 6, inside the blast furnace is present a transmission gradient which goes from values less than 0.1 at the top to values around 0.3–0.4 in the middle-low part. Indeed, in the fictitious cohesive zone that we manually inserted we detected an increase in the simulated flux of 13%±1% when we compare it to the uniform Fe density case.

4   Conclusions

The optimization of blast furnace operation through muography is presented as a new exciting and promising method. The results from this type of measurement can benefit steel production by improving the modelization of the internal structure. In particular, this knowledge can be used to stabilize the height and shape of the cohesive zone which is a key parameter during the reduction of the iron ore material. The installation process and the features of the BLEMAB project and detectors were highlighted and described concerning the first measurement campaign that started in August 2023.

While waiting for the processing of the experimental data, we tried to estimate throughout a first GEANT4 simplified simulation the possible effects of multiple scattering on the muographic measurement at blast furnaces. The results show how only a small percentage (around 5%) of the scattered muons have a significant impact on the muographic map. The two main effects are a blurring effect, which however is contained in the angular resolution, and a small overcounting of the muon counts around the edges of the object. The effect on the density map will be the next task to be performed. Moreover, we plan to implement a more complex CAD geometry of the blast furnace and cohesive zone in order to faithfully reproduce the experimental condition. The final goal will be to 3D reconstruct the zones of interest, predict new measuring points and implement also an online monitoring system for the blast furnace.

References

[1] Particle Data Group collaboration, *Review of Particle Physics*, *PTEP* **2022** (2022) 083C01.

[2] G. Bonomi et al., *Applications of cosmic-ray muons*, *Prog. Part. Nucl. Phys.* **112** (2020) 103768.

[3] L. Bonechi, R. D'Alessandro and A. Giammanco, *Atmospheric muons as an imaging tool*, *Rev. Phys.* **5** (2020) 100038 [arXiv:1906.03934].

[4] N. Su et al., *A Comparison of Muon Flux Models at Sea Level for Muon Imaging and Low Background Experiments*, *Front. Energy Res.* **9** (2021) 750159.

[5] L. Bonechi et al., *Development of the ADAMO detector: test with cosmic rays at different zenith angles*, in the proceedings of the *29th International Cosmic Ray Conference*, Pune, India, 3–10 August 2005, vol. 9, p. 283–286.

[6] D. Borselli et al., *Three-dimensional muon imaging of cavities inside the Temperino mine (Italy)*, *Sci. Rep.* **12** (2022) 22329.

[7] T. Beni et al., *Transmission-Based Muography for Ore Bodies Prospecting: A Case Study from a Skarn Complex in Italy*, *Nat. Resour. Res.* **32** (2023) 1529.

[8] G. Baccani et al., *The reliability of muography applied in the detection of the animal burrows within River Levees validated by means of geophysical techniques*, *J. Appl. Geophys.* **191** (2021) 104376.

[9] Y. Yang et al., *Chapter 1.1 — Ironmaking*, in *Treatise on Process Metallurgy. Volume 3: Industrial Processes*, S. Seetharaman ed., Elsevier (2014), p. 2–88 [DOI:10.1016/B978-0-08-096988-6.00017-1].

[10] BLEMAB collaboration, *BLEMAB European project: muon imaging technique applied to blast furnaces*, 2022 *JINST* **17** C04031 [arXiv:2110.10327].

[11] K. Nagamine et al., *Probing the inner structure of blast furnaces by cosmic-ray muon radiography*, *Proc. Japan Acad. B* **81** (2005) 257.

[12] A. Cohu et al., *First 3D reconstruction of a blast furnace using muography*, 2023 *JINST* **18** P07004 [arXiv:2301.04354].

[13] MURAVES collaboration, *The MURAVES Experiment: A Study of the Vesuvius Great Cone with Muon Radiography*, *J. Adv. Instrum. Sci.* **2022** (2022) 273 [arXiv:2202.12000].

[14] G. Baccani et al., *The MIMA project. Design, construction and performances of a compact hodoscope for muon radiography applications in the context of Archaeology and geophysical prospections*, 2018 *JINST* **13** P11001 [arXiv:1806.11398].

[15] J. Sauerwald et al., *Investigation of the coke network and cohesive zone by muon tomogrphy*, in the proceedings of the *42° Seminério de Redução de Minério de Ferro e Matérias-primas / 13° Seminário Brasileiro de Minério de Ferro / 6th International Congress on the Science and Technology of Ironmaking*, Rio de Janeiro, Brazil (2012), vol. 6, p. 1371–1378, ISSN: 2594-357X [DOI:10.5151/2594-357X-22237].

[16] A. Lechmann et al., *Muon tomography in geoscientific research — A guide to best practice*, *Earth Sci. Rev.* **222** (2021) 103842.

[17] GEANT4 collaboration, *GEANT4 — a simulation toolkit*, *Nucl. Instrum. Meth. A* **506** (2003) 250.

[18] V.N. Ivanchenko, O. Kadri, M. Maire and L. Urban, *Geant4 models for simulation of multiple scattering*, *J. Phys. Conf. Ser.* **219** (2010) 032045.

[19] A. Bagulya et al., *Recent progress of GEANT4 electromagnetic physics for LHC and other applications*, *J. Phys. Conf. Ser.* **898** (2017) 042032.

[20] J. Marteau et al., *Muons tomography applied to geosciences and volcanology*, *Nucl. Instrum. Meth. A* **695** (2012) 23 [arXiv:1201.6469].